

Dalton Transactions

Accepted Manuscript



This is an *Accepted Manuscript*, which has been through the Royal Society of Chemistry peer review process and has been accepted for publication.

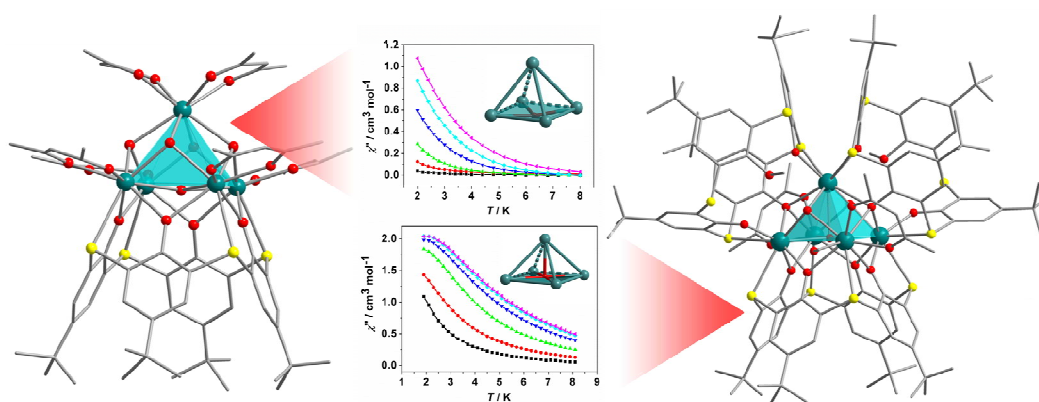
Accepted Manuscripts are published online shortly after acceptance, before technical editing, formatting and proof reading. Using this free service, authors can make their results available to the community, in citable form, before we publish the edited article. We will replace this *Accepted Manuscript* with the edited and formatted *Advance Article* as soon as it is available.

You can find more information about *Accepted Manuscripts* in the [Information for Authors](#).

Please note that technical editing may introduce minor changes to the text and/or graphics, which may alter content. The journal's standard [Terms & Conditions](#) and the [Ethical guidelines](#) still apply. In no event shall the Royal Society of Chemistry be held responsible for any errors or omissions in this *Accepted Manuscript* or any consequences arising from the use of any information it contains.

Graphic Abstract

A series of pentanuclear Ln^{III} clusters have been isolated based on thiacalix[4]arene and its derivatives for the first time. Detailed magnetic studies of all complexes reveal weak antiferromagnetic coupling among lanthanide metal ions. Two Dy_5 clusters feature different slow magnetic relaxation, which are affected presumably by the ligand field, molecular symmetry and coordination geometries of lanthanide ions.



Pentanuclear lanthanide pyramids based on thiacalix[4]arene ligand exhibiting slow magnetic relaxation

Jing-Yuan Ge,^a Jing Ru,^a Feng Gao,^{a,b} You Song,^a Xin-Hui Zhou,^c and Jing-Lin Zuo^{*a}

^a State Key Laboratory of Coordination Chemistry, School of Chemistry and Chemical Engineering, Collaborative Innovation Center of Advanced Microstructures, Nanjing University, Nanjing 210093, P. R. China

^b School of Chemistry and Chemical Engineering, Jiangsu Normal University, Xuzhou 221116, P. R. China

^c Institute of Advanced Materials, Nanjing University of Posts and Telecommunications, Nanjing 210046, P. R. China

Abstract

A series of pentanuclear Ln^{III} clusters, [Ln₅(μ₄-OH)(μ₃-OH)₄(L₁)(acac)₆] (H₄L₁ = *p*-*tert*-butylthiacalix[4]arene; acac = acetylacetonate; Ln = Dy, Ho, Er) and [Ln₅(μ₅-OH)(μ₃-OH)₄(L₁)(L₂)₂(acac)₂(CH₃OH)₂] (H₃L₂ = 5,11,17,23-tetrakis(1,1-dimethylethyl)-25,26,27-trihydroxy-28-methoxy thiacalix[4]arene; Ln = Dy, Ho, Er), have been synthesized based on thiacalix[4]arene ligand. All of these complexes feature a square-based pyramid with four triangular Ln₃ structural motifs. One μ₄-OH group bridges four Ln^{III} ions in the basal plane of **1–3**, while the OH group in complexes **4–6** adopts μ₅-coordination mode. Our results enrich the coordination modes of the versatile thiacalix[4]arene ligands and its application on new cluster compounds. The structural and magnetic studies confirm that molecular symmetries and coordination geometries for lanthanide metal cores have significant effect on some parameters as single-molecule magnets. Among them, two Dy₅ pyramids exhibit distinct slow magnetic relaxation.

* To whom correspondence should be addressed. Email: zuojl@nju.edu.cn; Fax: +86-25-83314502. Nanjing University.

Introduction

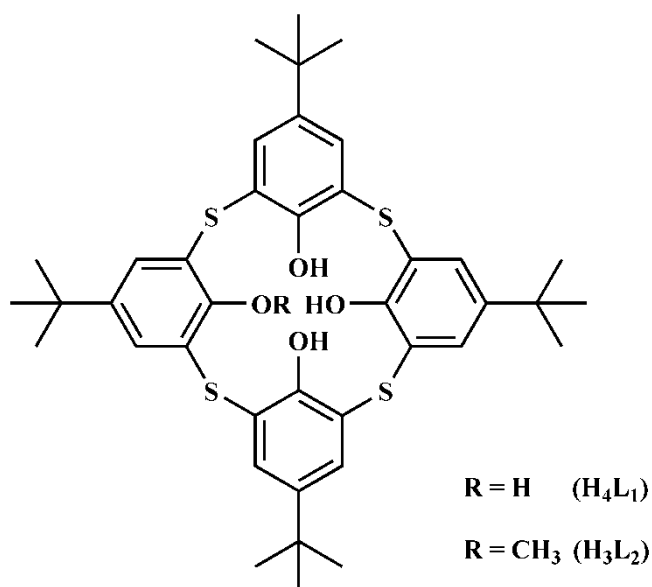
Single-molecule magnets (SMMs) have attracted considerable attention because of their appealing structures and functional applications in magnetic storage, molecular spintronics, and quantum computing, etc.¹ In particular, more and more lanthanide complexes have been reported since the discovery of $[\text{Tb}(\text{Pc})_2]^-$ ($\text{H}_2\text{Pc} =$ phthalocyanine).² In comparison with transition metal ions, lanthanide ions, especially Dy^{III} ion, usually exhibit high ground-state spin and large intrinsic magnetic anisotropy so that they can be regarded as good candidates for constructing new SMMs.³ Recently, some 4f-based polynuclear/high-nuclearity clusters,⁴ such as $[\text{Dy}_5(\mu_4\text{-OH})(\mu_3\text{-OH})_4(\text{Ph}_2\text{acac})_{10}]$ ($\text{Ph}_2\text{acac} =$ dibenzoylmethanide)^{4e} and $[\text{Dy}_5\text{O}(\text{O}i\text{Pr})_{13}]$,^{4f} are reported and they exhibit slow magnetic relaxation. With various ligand fields and coordination geometries of metal ions, they generally show distinct magnetic properties. Thus, synthesis of lanthanide polynuclear clusters in different topological structures, especially triangular Dy_3 structural motif⁵ that can produce unusual slow relaxation, is needed to illuminate the relationship between structures and properties of lanthanide SMMs.

However, the synthesis of 4f-based polynuclear SMMs is still a challenging task. The choice of suitable ligand plays a crucial role not only in the construction of polynuclears but also in tuning magnetic properties.^{3b,6} Our previous studies show that calix[4]arene derivatives, with multidentate coordination sites and rigid conformation, are good ligand candidates for the construction of mononuclear lanthanide SMMs.⁷

Following this idea, thiacalixarenes are particularly popular scaffolds for constructing a wealth of interesting polynuclear complexes, in that they can bond to some metal ions with four additional bridging sulfur atoms. So far, several thiacalix[4]arene-supported transition metal-based clusters and lanthanide-transition metal-based clusters have been obtained,⁸ but to the best of our knowledge, homometallic lanthanide clusters based on thiacalix[4]arene are rarely studied.⁹

Herein, for the first time, six lanthanide pentanuclear complexes, $[\text{Ln}_5(\mu_4\text{-OH})(\mu_3\text{-OH})_4(\text{L}_1)(\text{acac})_6] \cdot \text{Solv}$ ($\text{acac} =$ acetylacetonate; $\text{H}_4\text{L}_1 =$

p-*tert*-butylthiacalix[4]arene; **1**, Ln = Dy, Solv = 3CH₂Cl₂·CH₃OH·2H₂O; **2**, Ln = Ho, Solv = 3CH₂Cl₂·CH₃OH·H₂O; **3**, Ln = Er, Solv = 3CH₂Cl₂·CH₃OH·H₂O), and [Ln₅(μ₅-OH)(μ₃-OH)₄(L₁)(L₂)₂(acac)₂(CH₃OH)₂]·3acetone·2CH₃OH (H₃L₂ = 5,11,17,23-tetrakis(1,1-dimethylethyl)-25,26,27-trihydroxy-28-methoxy thiacalix[4]arene; **4**, Ln = Dy; **5**, Ln = Ho; **6**, Ln = Er), have been successfully synthesized based on the versatile thiacalix[4]arene ligand. The syntheses, crystal structures and magnetic properties are described in this paper. The results indicate that their magnetic properties are influenced by the inherent molecular symmetries, such as 4-fold symmetry, and the coordination geometries of metal cores.



Scheme 1

Experimental Section

Starting materials

All chemicals and solvents were obtained and used directly from the commercial sources. Starting materials, *p*-*tert*-butylthiacalix[4]arene ligand (H₄L₁) and one methylated ligand 5,11,17,23-tetrakis(1,1-dimethylethyl)-25,26,27-trihydroxy-28-methoxy thiacalix[4]arene (H₃L₂) (Scheme 1), were prepared according to the published literatures.¹⁰

Syntheses

[Dy₅(μ₄-OH)(μ₃-OH)₄(L₁)(acac)₆]·3CH₂Cl₂·CH₃OH·2H₂O (1). The thiacalix[4]arene ligand H₄L₁ (0.15 g, 0.20 mmol) and Dy(acac)₃·2H₂O (0.50 g, 1.00 mmol) were dissolved in toluene (4 mL). The reaction mixture was refluxed for 24 h, and then cooled to the room temperature. After the resulting solid was filtered, it was dissolved in 6 mL of CH₂Cl₂/CH₃OH (1:1 v/v). The solutions were left for about five days at room temperature, and colorless block-shaped crystals of **1** were obtained. Yield, 58%. Elemental analysis (%) calcd for [Dy₅(μ₄-OH)(μ₃-OH)₄(L₁)(acac)₆]·2H₂O (C₇₀H₉₅Dy₅O₂₃S₄): C 37.31, H 4.25, S 5.68. Found: C, 37.15, H, 4.37, S 5.61. Selected IR (KBr pellet, cm⁻¹): 3633 (w), 3441 (br), 2962 (m), 1600 (s), 1518 (s), 1458 (s), 1386 (s), 1309 (m), 1264 (m), 1018 (m), 921 (w), 879 (w), 839 (w), 654 (m), 531 (m).

[Ho₅(μ₄-OH)(μ₃-OH)₄(L₁)(acac)₆]·3CH₂Cl₂·CH₃OH·H₂O (2). The procedure was similar to the synthesis of **1** except that Ho(acac)₃·2H₂O was used in place of Dy(acac)₃·2H₂O. The pink block-shaped crystals of **2** were obtained. Yield, 62%. Elemental analysis (%) calcd for [Ho₅(μ₄-OH)(μ₃-OH)₄(L₁)(acac)₆]·H₂O (C₇₀H₉₃Ho₅O₂₂S₄): C 37.54, H 4.19, S 5.73. Found: C, 37.29, H, 4.24, S 5.67. Selected IR (KBr pellet, cm⁻¹): 3441 (br), 2962 (m), 1600 (s), 1518 (vs), 1461 (s), 1386 (s), 1310 (m), 1265 (m), 1019 (w), 922 (w), 839 (w), 752 (w), 655 (w), 532 (m).

[Er₅(μ₄-OH)(μ₃-OH)₄(L₁)(acac)₆]·3CH₂Cl₂·CH₃OH·H₂O (3). The procedure was similar to the synthesis of **1** except that Er(acac)₃·2H₂O was used in place of Dy(acac)₃·2H₂O. The pink block-shaped crystals of **3** were obtained. Yield, 65%. Elemental analysis (%) calcd for [Er₅(μ₄-OH)(μ₃-OH)₄(L₁)(acac)₆]·H₂O (C₇₀H₉₃Er₅O₂₂S₄): C 37.45, H 4.18, S 5.70. Found: C, 37.16, H 4.30, S 5.65. Selected IR (KBr pellet, cm⁻¹): 3634 (w), 3426 (br), 2962 (m), 1600 (s), 1518 (s), 1463 (s), 1386 (s), 1311 (m), 1262 (m), 1019 (w), 922 (w), 839 (w), 801 (w), 657 (w), 533 (w).

[Dy₅(μ₅-OH)(μ₃-OH)₄(L₁)(L₂)₂(acac)₂(CH₃OH)₂]·3acetone·2CH₃OH (4). The thiacalix[4]arene ligand H₄L₁ (14.4 mg, 0.02 mmol), one methylated thiacalix[4]arene ligand H₃L₂ (14.7 mg, 0.02 mmol), and Dy(acac)₃·2H₂O (9.2 mg, 0.02 mmol) were dissolved in 10 mL of acetone/methanol (1:1 v/v). The reaction mixture was stirred and heated at 85 °C for 24 h, and then cooled to the room temperature. Colorless

block-shaped crystals of **4** were obtained. Yield, 20%. Elemental analysis (%) calcd for $[\text{Dy}_5(\mu_5\text{-OH})(\mu_3\text{-OH})_4(\text{L}_1)(\text{L}_2)_2(\text{acac})_2(\text{CH}_3\text{OH})_2]$ ($\text{C}_{134}\text{H}_{163}\text{Dy}_5\text{O}_{21}\text{S}_{12}$): C 48.56, H 4.96, S 11.59. Found: C, 48.88, H, 5.04, S 11.55. Selected IR (KBr pellet, cm^{-1}): 3446 (br), 2962 (m), 2360 (w), 1589 (m), 1522 (m), 1452 (s), 1380 (m), 1302 (m), 1256 (m), 1121 (w), 1090 (w), 1019 (w), 875 (w), 837 (w), 736 (w).

$[\text{Ho}_5(\mu_5\text{-OH})(\mu_3\text{-OH})_4(\text{L}_1)(\text{L}_2)_2(\text{acac})_2(\text{CH}_3\text{OH})_2] \cdot 3\text{acetone} \cdot 2\text{CH}_3\text{OH}$ (5). The procedure was similar to the synthesis of **4** except that $\text{Ho}(\text{acac})_3 \cdot 2\text{H}_2\text{O}$ was used in place of $\text{Dy}(\text{acac})_3 \cdot 2\text{H}_2\text{O}$. The pink block-shaped crystals of **5** were obtained. Yield, 26%. Elemental analysis (%) calcd for $[\text{Ho}_5(\mu_5\text{-OH})(\mu_3\text{-OH})_4(\text{L}_1)(\text{L}_2)_2(\text{acac})_2(\text{CH}_3\text{OH})_2]$ ($\text{C}_{134}\text{H}_{163}\text{Ho}_5\text{O}_{21}\text{S}_{12}$): C 48.49, H 4.95, S 11.59. Found: C, 48.66, H, 5.09, S 11.27. Selected IR (KBr pellet, cm^{-1}): 3447 (br), 2962 (m), 2360 (w), 1589 (m), 1522 (m), 1453 (s), 1380 (m), 1303 (m), 1257 (m), 1122 (w), 1090 (w), 1019 (w), 875 (w), 838 (w), 737 (w).

$[\text{Er}_5(\mu_5\text{-OH})(\mu_3\text{-OH})_4(\text{L}_1)(\text{L}_2)_2(\text{acac})_2(\text{CH}_3\text{OH})_2] \cdot 3\text{acetone} \cdot 2\text{CH}_3\text{OH}$ (6). The procedure was similar to the synthesis of **4** except that $\text{Er}(\text{acac})_3 \cdot 2\text{H}_2\text{O}$ was used in place of $\text{Dy}(\text{acac})_3 \cdot 2\text{H}_2\text{O}$. The pink block-shaped crystals of **6** were obtained. Yield, 34%. Elemental analysis (%) calcd for $[\text{Er}_5(\mu_5\text{-OH})(\mu_3\text{-OH})_4(\text{L}_1)(\text{L}_2)_2(\text{acac})_2(\text{CH}_3\text{OH})_2]$ ($\text{C}_{134}\text{H}_{163}\text{Er}_5\text{O}_{21}\text{S}_{12}$): C 48.41, H 4.95, S 11.55. Found: C, 48.07, H, 5.13, S 11.85. Selected IR (KBr pellet, cm^{-1}): 3446 (br), 2962 (s), 2360 (w), 1590 (m), 1523 (m), 1453 (s), 1380 (m), 1303 (m), 1257 (m), 1122 (w), 1090 (w), 1018 (w), 875 (w), 838 (w), 737 (w).

X-ray Structure Determination. The crystal structures were determined on a Bruker Smart Apex II CCD-based diffractometer (Mo $K\alpha$ radiation, $\lambda = 0.71073 \text{ \AA}$). The raw frame data were integrated into SHELX-format reflection files and corrected for Lorentz and polarization effects using SAINT.¹¹ Corrections for incident and diffracted beam absorption effects were applied using SADABS supplied by Bruker.¹² None of the crystals showed evidence of crystal decay during data collection. All structures were solved and refined against F^2 by the full-matrix least-squares using the SHELXL-97 program.¹³ The positions of the metal atoms and their first coordination spheres were located from direct method E-maps. All non-hydrogen atoms were

refined with anisotropic thermal parameters, and hydrogen atoms of the organic ligands and the hydroxide anion were calculated theoretically onto the specific atoms and refined isotropically with fixed thermal factors. A number of restraints were applied owing to disorder in solvent molecules and the *p-tert*-butyl groups of thiacalix [4] ligands. It was very difficult to model reliably all the mixed solvent molecules in complexes **4–6**. Therefore, some contributions of the electron density from the remaining solvent molecules were removed by the SQUEEZE routine in PLATON.¹⁴ More details for the crystal data, data collection parameters, and refinement statistics were given in Table 1. Relevant interatomic bond distances and bond angles were listed in Tables S1 and S2. CCDC reference numbers 1062207 (**1**), 1062208 (**2**), 1062209 (**3**), 1062210 (**4**), 1062211(**5**), 1062212 (**6**).

Physical Measurements. Elemental analyses were performed on a Elementar Vario MICRO analyzer. Infrared (IR) samples were prepared as KBr pellets, and spectra were obtained in the 400-4000 cm⁻¹ range using a Vector22 Bruker spectrophotometer. XRD patterns were obtained on a D8 ADVANCE X-ray powder diffractometer (XRPD) with Cu K α radiation ($\lambda = 1.5405 \text{ \AA}$). Magnetic susceptibility measurements for **1–6** were measured with the use of a Quantum Design MPMS-SQUID-VSM magnetometer in the temperature range 1.9–300 K. Field dependences of magnetization were measured using Quantum Design MPMS-SQUID-VSM system in an applied field up to 70 kOe.

Results and discussion

Synthesis and Characterizations

Thiacalix[4]arene and its derivatives have been proven to be possible for the construction of polynuclear lanthanide clusters.⁹ The reactions of H₄L₁ and Ln(acac)₃·2H₂O in toluene solution resulted into the formation of complexes **1–3**. Suitable single crystals were obtained by the slow evaporation of the mixed solution (dichloromethane/methanol) containing the resulting product. However, it is difficult

to control the partial deprotonation of phenolic hydroxyl groups in thiacalix[4]arene. The alkylation of phenolic hydroxyl groups seems to be a better way to control charge of the ligand.^{7,15} Additionally, the self-assembly based on some mixed ligands may give new and fascinating structure.¹⁶ With these in mind, H₃L₂ was introduced in the preparation of lanthanide clusters. Indeed, complexes **4–6** were successfully constructed after solvothermal reactions between mixed ligands (H₄L₁ and H₃L₂) and Ln(acac)₃·2H₂O in methanol and acetone. The XRPD experimental and simulated patterns of complexes **1–6** are shown in the Supporting Information (Fig. S1)†, confirming the purity of the bulk synthesized materials. The protonation level of the OH groups in complexes **1–6** was determined by charge balance considerations and bond valence sum (BVS) calculations.¹⁷

Structural Description

The X-ray crystal structure analysis revealed that **1–3** are isostructural (Fig. S2, ESI)†, taking complex **1** as an example to describe the structure in detail. Complex **1** crystallizes in the triclinic *P* $\bar{1}$ space group. The asymmetric unit contains five crystallographic Dy^{III} ions, as shown in Fig. 1, all Dy^{III} ions are eight-coordinated. Dy1, Dy2, Dy3 and Dy4 ions are in the same {DyO₇S} coordination environment, while Dy5 ion, features a {DyO₈} coordination sphere. All S atoms (S1, S2, S3 and S4) are attributed to the thiacalix[4]arene ligand (L₁) with the Dy–S distances in the range of 2.926–2.964 Å. The coordinated O atoms fall into four groups: every phenolic O atoms (O1–O4) of L₁ forms a μ - η^2 -bridge along one of the edges of the square basal plane; the μ_4 -O5 atom (from OH) links four basal Dy^{III} ions together to form a Dy₄(μ_4 -OH) unit; every μ_3 -hydroxo O atoms (O6–O9) from OH groups bridges each of the four triangular face; the terminal ketonate O atoms (O10–O21) from six bidentate acac anions embrace the Dy₅ pyramid. The Dy–O_{ketonate} distances (2.249–2.341 Å) are little shorter than Dy–O_{phenoxo} distances, which fall in the range of 2.318–2.373 Å. However, all Dy–O and Dy–S bond lengths (Table S1)† are within the normal range according to the previous reports.¹⁸

The arrangement of these five Dy^{III} ions may best be described as a square-based pyramid, similar to [Dy₅(μ₄-OH)(μ₃-OH)₄(Ph₂acac)₁₀].^{4e} Dy1, Dy2, Dy3 and Dy4 ions locate the basal plane with the dihedral angles between every two planes, created by three neighbouring Dy^{III} ions (plane 1 (Dy1, Dy2, Dy3), plane 2 (Dy2, Dy3, Dy4), plane 3 (Dy3, Dy4, Dy1) and plane 4 (Dy4, Dy1, Dy2)), in the range of 0.110°-0.157° and the average value is 0.126°. Within the basal Dy₄(μ₄-OH) unit, the average distance between the adjacent Dy^{III} ions is 3.538 Å and the Dy–Dy–Dy angle fall in the range of 89.41–90.59°. Moreover, the diagonal metal distances linked by μ₄-OH (O5) are 4.982 and 5.023 Å and the average Dy–O5 bond length is 2.512 Å. It is noted that O5 atom is separated from apical Dy5 ion with a long distance of 3.046 Å, which is too longer to be considered as Dy–O bond.^{18b} Further analyses show that the square-based pyramid is much elongated, with the average distance between the apical Dy5 and the basal Dy^{III} ions is 3.766 Å (see Table S1 for details)†, which is much longer than 3.538 Å in the basal plane. The vertical distance between apical Dy5 ion and the square plane is 2.816 Å.

The solvated molecules (including three CH₂Cl₂, one CH₃OH and two H₂O) are found around the Dy₅ cluster. There are several weak hydrogen-bonding interactions between the solvent and host framework, as shown in Fig. S3a.† Moreover, the neighboring Dy₅ clusters further link to each other with regular head-to-tail orientation along the *b* axis *via* C–H⋯Cl and C–H⋯O non-classical hydrogen bonds (Table S3)†. These ⋯Dy₅⋯Dy₅⋯Dy₅⋯ chains extend to form a layer in the *bc* plane through two sets of C–H⋯π interactions, with the shortest interchain Dy⋯Dy distance of 8.985 Å (Fig. S3b and S3c)†. In the solid state, every layers stack to each other in an ⋯ABAB⋯ fashion and there are no significant interlayer interactions have been found (Fig. 1c).

In the presence of H₃L₂ ligand, the reaction of H₄L₁ and Ln(acac)₃ in a mixed-solvent system (methanol/acetone) gives the pyramidal complexes **4–6**. The X-ray crystal structure analyses reveal that **4–6** are isostructural (Fig. S4)†. Only complex **4** will be described here. The asymmetric unit contains one Dy₅ cluster, which is capped by one L₁ ligand, two L₂ ligands, two bidentate acac anions and two

coordinated CH₃OH molecules (Fig. 2a). As shown in Fig. 2b, these five Dy^{III} ions have different coordination spheres. Dy1 and Dy3 adopt eight-coordinated {DyO₆S₂} environment, Dy2 and Dy4 lie in nine-coordinated {DyO₈S} sphere, while Dy5 features a distorted tricapped trigonal prismatic geometry {DyO₇S₂}. Two fully deprotonated L₂ ligands adopt similar coordination mode, which has not been reported previously. All S atoms are contributed to one L₁ (S5, S6, S7 and S8) and two L₂ (S2 and S3 from one L₂, S10 and S11 from the other one), with the Dy–S bond lengths in the range of 2.879 Å–3.045 Å. The bowl-shaped conformation of L₁, in which each of phenolic O atoms (O5, O6, O7 and O8) adopts a μ - η^2 -bridge mode, is the same as that in **1**. Two L₂ ligands also process bowl-shaped conformation. However, four phenolic O atoms of L₂ (O1, O2, O3 and O4 from one L₂, O9, O10, O11 and O12 from the other one) adopt three different bonding modes: O1 (or O12) atom from methoxy group is uncoordinated; O3 (O10) atom forms μ_3 -bridge, located at one triangular face of the square-based pyramid; O2 (O9) and O4 (O11) atoms are monodentate to link one basal Dy3 ion (Dy1) and the apical Dy5 ion, respectively. The other two triangular faces of the pyramid are capped by two μ_3 -O atoms (O14 and O15) from OH groups, which link to uncoordinated O1 (or O12) *via* O–H \cdots O hydrogen bond (Fig. S5)†. Finally, Dy2 (Dy4) ion is also capped by three O atoms from one bidentate acac anion (O16 and O17 for Dy4, O19 and O20 for Dy2) and one CH₃OH molecule (O18 for Dy4, O21 for Dy2), respectively. The average Dy–O_{CH₃OH} bond length is 2.432 Å, which is slightly longer than the average Dy–O_{acac} bond length of 2.295 Å (Table S2)†. However, all Dy–O bond lengths (2.184–2.761 Å) are within the range of normal values.

The configuration of Dy₅ cluster can also be considered as a square-based pyramid. Dy1, Dy2, Dy3 and Dy4 ions locate in the basal plane of the pyramid, and the average dihedral angle (calculated in the same way as it in **1**) is 1.106°, which is much bigger than 0.126° in **1**. Further analyses show that the structure of Dy₅ cluster in **4** is rather different from that in **1**. Within the basal plane, the average distance between the adjacent Dy^{III} ions is 3.659 Å (see Table S2 for details)†, while the average distance between Dy5 and the basal Dy^{III} ions is 3.671 Å. Compared with **1**, it is clear that

pyramid in **4** is slightly compressed, due to the existence of μ_5 -O13 atom probably. O13 atom adopts μ_5 -coordination mode rather than the μ_4 -coordination mode of O5 in **1**, to link five Dy^{III} ions together. The μ_5 -O13 atom lies in the center of the square basal plane, and the bond length of Dy5–O13 is 2.578 Å, approximately equal to the average Dy–O bond length (2.583 Å) within the basal plane, which is much shorter than the distance of Dy5···O5 in **1** (3.049 Å). The difference in coordination geometries may play an influential role in magnetic properties.

Three solvated acetone and two solvated CH₃OH molecules exist around the Dy₅ cluster. The CH₃OH molecules are weakly connected by O–H···O hydrogen bonds (Table S3)†, as shown in Fig. S5.† In the solid state, neighboring Dy₅ clusters stack together in an ...ABAB... fashion along the *ac* plane (Fig. 2c). Uncoordinated solvent fills the interstices. There are no interactions between the neighbouring molecules, with the shortest intermolecular Dy···Dy distance of 11.344 Å.

Magnetic Properties

Magnetic susceptibility measurements on fresh samples for complexes **1–6** were performed in the temperature range 2–300 K under an applied magnetic field of 1000 Oe. The $\chi_M T$ values at room temperature are 71.42, 69.88 and 55.75 cm³ K mol⁻¹ for **1**, **2** and **3**, respectively (Fig. 3a), while the $\chi_M T$ values for complexes **4–6** are 70.60, 70.43 and 56.98 cm³ K mol⁻¹, respectively (Fig. 3b). All of them are consistent with the theoretical values for five uncoupled Ln^{III} ions (70.83 cm³ K mol⁻¹ for Dy^{III}, ⁶H_{15/2}, $J = 15/2$, $g = 4/3$; 70.31 cm³ K mol⁻¹ for Ho^{III}, ⁵I₈, $J = 8$, $g = 5/4$; 57.38 cm³ K mol⁻¹ for Er^{III}, ⁴I_{15/2}, $J = 15/2$, $g = 6/5$). As the temperature decreases, each $\chi_M T$ value decreases gradually and then drops rapidly in the lower temperature region to a minimum value of 23.43, 16.72, 26.44, 27.62, 27.38 and 27.50 cm³ K mol⁻¹ for **1–6**, respectively, at 2.0 K. This result may mainly be due to the thermal depopulation of the Ln^{III} ions excited Stark sublevels.^{6a} Because of the orbital contribution, the magnetic properties of all complexes cannot be fitted for determining the coupling mode. For roughly estimating the coupling between metal ions, their magnetic properties such as $\chi_M T$ values at lowest temperature are compared to that of

mononuclear complex.¹⁹ One fifth of the $\chi_{\text{M}}T$ values of **1–6** are much lower than the single-ion values in the non-interacting complexes reported previously,²⁰ suggesting antiferromagnetic coupling between lanthanide ions.¹⁹ At 1.9 K and 70 kOe, the magnetizations (M) against field (H) reach 27.84, 25.38, 21.86 $N\beta$ for **1–3**, and 26.80, 24.77, 24.01 $N\beta$ for **4–6**, respectively (Fig. 4), in agreement with expected values. The lack of expected saturation values is most likely due to the presence of magnetic anisotropy and/or the effects of low-lying excited states.²¹

The alternating current (ac) magnetic susceptibility under $H_{\text{ac}} = 2$ Oe were performed for all of the complexes to check for any SMM behavior. Under zero and optimized external dc field (1000 Oe), two Dy complexes (**1** and **4**) show obvious in-phase signals (χ') and out-of-phase signals (χ'') of the ac susceptibility, suggesting the presence of an activated relaxation process.²² In the case of Ho (**2** and **5**) and Er (**3** and **6**) complexes, however, no χ'' signals were observed at neither zero dc field nor 1000 Oe dc field (Fig. S10-13)†.

For complex **1**, the temperature-dependent ac susceptibility measurements under zero dc field in the frequency range 1–999 Hz are depicted in Fig. 5. The obvious “tails” of out-of-phase (χ'') signal at low temperature reveals the slow relaxation of the magnetization, typical of SMM behavior. However, the maximum of χ'' for **1** was not observed even up to 999 Hz, and the energy barrier or characteristic relaxation time of **1** cannot be obtained according to the Arrhenius law. When an external dc field (1000 Oe) was introduced, the ac signals are also not observed (Fig. S6)†. The high-frequency χ'' susceptibility is higher than the low-frequency one, implying that the peak maxima are to be found below the minimum operating temperature or the maximum frequency of our SQUID instrument. These results show that the χ'' signal at low temperature may be due to the presence of fast zero-field magnetic relaxation, usually seen in 4f-based SMMs.^{4e,23} Furthermore, variable-frequency ac susceptibilities under zero and 1000 Oe dc field have not detected full peaks even at the lowest temperature 1.9 K (Fig. S7)†.

For **4**, the temperature-dependent ac susceptibility measurements under zero and 1000 Oe dc field reveal frequency dependent χ' and χ'' signals. Both χ' and χ'' signals

have no clear peaks under both zero (Fig. 6) and 1000 Oe (Fig. S8)† dc field as same as ones in **1**. However, χ'' signals of **4** show a relatively slow increase at the low temperature region and have a tendency of peaks that is different from **1**. Frequency-dependent ac susceptibility measurements were also performed under both zero and 1000 Oe dc field, as shown in Fig. S9.† Under zero dc field, the maximum of χ'' was not observed even at the lowest temperature 1.9 K from 1 Hz to 999 Hz. At 1.9 K, although χ'' values increase gently at the high frequencies under 1000 Oe dc field, no clearly peak was detected. Combining temperature- and frequency-dependent ac susceptibility measurements shows that the application of external field has no effect on the dynamics above 1.9 K. We think the slow magnetic relaxation of **4** at low temperature also might be attributed to the presence of fast zero-field magnetic relaxation.

Compared **1** with **4**, although both of them feature pyramids with triangular Dy₃ structural motifs, however, different dynamic magnetic properties are found for them. To understand this, some important structural parameters are summarized and analyzed in Table 2. One crucial reason resulting in the different dynamic behaviors between **1** and **4** is from the central O atoms, which adopt μ_4 - or μ_5 -bridge modes in **1** and **4**, respectively. As for [Dy₅O(OiPr)₁₃] and [Tb(Pc)₂]⁻ complexes, four-fold symmetry seem to be very important. In addition, the dynamic magnetic behaviors for 4f-based SMMs are closely related to the inherent symmetry and coordination geometry of the central metal cores.^{6b} Further analyses of the geometry of Dy^{III} ions are determined by SHAPE 2.1 software. Tables S4 and S5 show, in **1**, four Dy^{III} ions in the basal plane and one apical Dy^{III} ion are ascribed to approximate local biaugmented trigonal prism J50 (C_{2v}) symmetry and square antiprism (D_{4d}) symmetry, respectively. On the case of **4**, two eight-coordinated Dy^{III} ions and two nine-coordinated Dy^{III} ions in the basal plane lie in four different symmetries, snub diphendoid J84 (D_{2d}), triangular dodecahedron (D_{2d}) symmetry, capped square antiprism J10 (C_{4v}) and spherical capped square antiprism (C_{4v}) symmetries, respectively, while the apical Dy^{III} ion is tricapped trigonal prism J51 (D_{3h}) symmetry. Different symmetry produces unusual effect on the dynamic behaviors of **1** and **4**. As

we all know, the magnetic properties of only two Dy₅ square-based pyramids^{4e,4f} have been reported. (The magnetic measurement of [Dy₅(μ₄-OH)(μ₃-OH)₄(IPhacac)₁₀] (IPhacac = bis(*para*-iododibenzoyl)-methanide) has not been performed).²⁴ One is [Dy₅(μ₄-OH)(μ₃-OH)₄(Ph₂acac)₁₀], crystallized in the tetragonal *P4/n* space group and contained five {DyO₈} eight-coordinated metal ions. Comparing **1** with the similar [Dy₅(μ₄-O)] family member [Dy₅(μ₄-OH)(μ₃-OH)₄(Ph₂acac)₁₀], the strength of the ligand field and the molecular local symmetry are key factors in the slow magnetic relaxation in lanthanide polynuclear SMMs. In **1**, Dy^{III} ions are eight-coordinated completed by O and S atoms, the ligand field is probably too strong to change the intrinsic characteristics of lanthanide ions. The other is [Dy₅O(O*i*Pr)₁₃], which has five {DyO₆} six-coordinated metal ions in octahedron (*O_h*) symmetry. The magnetic property of **4** is not better than [Dy₅O(O*i*Pr)₁₃] with slow magnetic relaxation to 40 K may be attributed to not only the strength of the ligand field but also multiple coordination modes of central Dy^{III} ions.

Conclusions

In summary, six lanthanide pentanuclear clusters have been isolated with the introduction of thiacalix[4]arene as the chelating ligand. The forgoing results enrich the coordination chemistry for the versatile thiacalix[4]arene ligands. Magnetic studies of all complexes reveal weak antiferromagnetic coupling among lanthanide metal ions. Among them, frequency dependent χ'' signals are observed for two Dy₅ pyramids (**1** and **4**), which may result from the presence of fast zero-field magnetic relaxation. Comparison between these two complexes and the Dy₅ family members in previously reported literature suggests that the dynamic behaviors are affected presumably by the ligand field and molecular symmetry and coordination geometry of lanthanide ion. To understand the inner and essential relationship between structures and magnetic properties of the type of polynuclear lanthanide complexes, more works on similar systems are underway in our laboratory.

Acknowledgments

This work was supported by the Major State Basic Research Development Program (2011CB808704 and 2013CB922101), the National Natural Science Foundation of China (51173075 and 21401085), the Natural Science Foundation of Jiangsu Province (BK20130054). We also thank Jia-Ze Xie and Zhuang-Yu Zhao for experimental assistance on the preparation of ligands, and Prof. Yan Xu from Nanjing University of Technology for structural analyses.

Supporting Information

Additional structures, XRPD patterns, magnetic characterizations and X-ray crystallographic files in CIF format for all complexes. This material is available free of charge via the Internet at <http://www.rsc.org>.

References

- 1 (a) R. Sessoli, H. -L. Tsai, A. R. Schake, S. Wang, J. B. Vincent, K. Folting, D. Gatteschi, G. Christou, D. N. Hendrickson, *J. Am. Chem. Soc.*, 1993, **115**, 1804; (b) R. Sessoli, D. Gatteschi, A. Caneschi, M. A. Novak, *Nature*, 1993, **365**, 141. (c) F. Troiani, M. Affronte, *Chem. Soc. Rev.*, 2011, **40**, 3119; (d) M. Andruh, J. P. Costes, C. Diaz, S. Gao, *Inorg. Chem.*, 2009, **48**, 3342; (e) Y. Horii, K. Katoh, N. Yasuda, B. K. Breedlove, M. Yamashita, *Inorg. Chem.*, 2015, **54**, 3297; (f) S. Titos-Padilla, J. Ruiz, J. M. Herrera, E. K. Brechin, W. Wersndorfer, F. Lloret, E. Colacio, *Inorg. Chem.*, 2013, **52**, 9620; (g) K. R. Meihaus, J. R. Long, *J. Am. Chem. Soc.*, 2013, **135**, 17952.
- 2 N. Ishikawa, M. Sugita, T. Ishikawa, S. Y. Koshihara, Y. Kaizu, *J. Am. Chem. Soc.*, 2003, **125**, 8694.
- 3 (a) H. L. C. Feltham, S. Brooker, *Coord. Chem. Rev.*, 2014, **276**, 1; (b) D. N. Woodruff, R. E. Winpenny, R. A. Layfield, *Chem. Rev.*, 2013, **113**, 5110; (c) K. R. Meihaus, S. G. Minasian, W. W. Jr. Lukens, S. A. Kozimor, D. K. Shuh, T. Tyliczszak, J. R. Long, *J. Am. Chem. Soc.*, 2014, **136**, 6056; (d) P. Zhang, L. Zhang,

- J.-K. Tang, *Dalton Trans.*, 2015, **44**, 3923.
- 4 (a) Y.-N. Guo, G.-F. Xu, W. Wernsdorfer, L. Ungur, Y. Guo, J.-K. Tang, H.-J. Zhang, L. F. Chibotaru, A. K. Powell, *J. Am. Chem. Soc.*, 2011, **133**, 11948; (b) K. Suzuki, R. Sato, N. Mizuno, *Chem. Sci.*, 2013, **4**, 596; (c) L. F. Chibotaru, L. Ungur, A. Soncini, *Angew. Chem. Int. Ed.*, 2008, **120**, 4194; (d) M. U. Anwar, L. K. Thompson, L. N. Dawe, F. Habib, M. Murugesu, *Chem. Commun.*, 2012, **48**, 4576; (e) M. T. Gamer, Y. Lan, P. W. Roesky, A. K. Powell, R. Clerac, *Inorg. Chem.*, 2008, **47**, 6581; (f) R. J. Blagg, C. A. Muryn, E. J. McInnes, F. Tuna, R. E. Winpenny, *Angew. Chem. Int. Ed.*, 2011, **50**, 6530; (g) T. Kajiwarra, K. Katagiri, M. Hasegawa, A. Ishii, M. Ferbinteanu, S. Takaishi, T. Ito, M. Yamashita, N. Iki, *Inorg. Chem.*, 2006, **45**, 4880; (h) S. K. Langley, N. F. Chilton, I. A. Gass, B. Moubaraki, K. S. Murray, *Dalton Trans.*, 2011, **40**, 12656; (i) J. W. Sharples, Y. Z. Zheng, F. Tuna, E. J. McInnes, D. Collison, *Chem. Commun.*, 2011, **47**, 7650; (j) H.-H. Zou, R. W., Z.-L. Chen, D.-C. Liu, F.-P. Liang, *Dalton Trans.*, 2014, **43**, 2581; (k) M.-Y. Wu, F.-L. Jiang, D.-Q. Yuan, J.-D. Pang, J.-J. Qian, S. A. Al-Thabaitic, M.-C. Hong, *Chem. Commun.*, 2014, **50**, 1113; (l) M.-Y. Wu, F.-L. Jiang, X.-J. Kong, D.-Q. Yuan, L.-S. Long, S. A. Al-Thabaitic, M.-C. Hong, *Chem. Sci.*, 2013, **4**, 3104; (m) L. X. Chang, G. Xiong, L. Wang, P. Cheng, B. Zhao, *Chem. Commun.*, 2013, **49**, 1055.
- 5 (a) I. J. Hewitt, J.-K. Tang, N. T. Madhu, C. E. Anson, Y. Lan, J. Luzon, M. Etienne, R. Sessoli, A. K. Powell, *Angew. Chem. Int. Ed.*, 2010, **49**, 6352; (b) J.-K. Tang, I. Hewitt, N. T. Madhu, G. Chastanet, W. Wernsdorfer, C. E. Anson, C. Benelli, R. Sessoli, A. K. Powell, *Angew. Chem. Int. Ed.*, 2006, **45**, 1729.
- 6 (a) W.-B. Sun, B.-L. Han, P.-H. Lin, H.-F. Li, P. Chen, Y.-M. Tian, M. Murugesu, P.-F. Yan, *Dalton Trans.*, 2013, **42**, 13397; (b) L. Sorace, C. Benelli, D. Gatteschi, *Chem. Soc. Rev.*, 2011, **40**, 3092; (c) W.-B. Sun, B. Yan, Y.-Q. Zhang, B.-W. Wang, Z.-M. Wang, J.-H. Jia, S. Gao, *Inorg. Chem. Front.*, 2014, **1**, 503.
- 7 F. Gao, L. Cui, Y. Song, Y.-Z. Li, J.-L. Zuo, *Inorg. Chem.*, 2014, **53**, 562.
- 8 (a) Y.-F. Bi, S.-C. Du, W.-P. Liao, *Coord. Chem. Rev.*, 2014, **276**, 61; (b) K.-C. Xiong, F.-L. Jiang, Y.-L. Gai, Z.-C. He, D.-Q. Yuan, L. Chen, K.-Z. Su, M.-C.

- Hong, *Cryst. Growth Des.*, 2012, **12**, 3335; (c) Y.-F. Bi, S.-C. Du, W.-P. Liao, *Chem. Commun.*, 2011, **47**, 4724; (d) K.-C. Xiong, X.-Y. Wang, F.-L. Jiang, Y.-L. Gai, W.-T. Xu, K.-Z. Su, X.-J. Li, D.-Q. Yuan, M.-C. Hong, *Chem. Commun.*, 2012, **48**, 7456; (e) K.-Z. Su, F.-L. Jiang, J.-J. Qian, M.-Y. Wu, K.-C. Xiong, Y.-L. Gai, M.-C. Hong, *Inorg. Chem.*, 2013, **52**, 3780; (f) K.-Z. Su, F.-L. Jiang, J.-J. Qian, L. Chen, J.-D. Pang, S. M. Bawaked, M. Mokhtar, S. A. Al-Thabaiti, M.-C. Hong, *Inorg. Chem.*, 2015, **54**, 3183.
- 9 (a) Y.-F. Bi, X.-T. Wang, W.-P. Liao, X.-W. Wang, R.-P. Deng, H.-J. Zhang, S. Gao, *Inorg. Chem.*, 2009, **48**, 11743; (b) A. Bilyk, A. K. Hall, J. M. Harrowfield, M. W. Hosseini, B. W. Skelton, A. H. White, *Aust. J. Chem.*, 2000, **53**, 895.
- 10 (a) N. Iki, C. Kabuto, T. Fukushima, H. Kumagai, H. Takeya, S. Miyanari, T. Miyashi, S. Miyano, *Tetrahedron*, 2000, **56**, 1437; (b) *JP Pat.*, 10168078, 1998.
- 11 *SAINT-Plus*, version 6.02; Bruker Analytical X-ray System: Madison, WI, 1999.
- 12 G. M. Sheldrick, *SADABS an empirical absorption correction program*; Bruker Analytical X-ray Systems: Madison, WI, 1996.
- 13 G. M. Sheldrick, *SHELXTL-97*; Universität of Göttingen: Göttingen, Germany, 1997.
- 14 Platon Program: A. L. Spek, *Acta Cryst. Sect. A.*, 1990, **46**, 194.
- 15 R. Kumar, Y. O. Lee, V. Bhalla, M. Kumar, J. S. Kim, *Chem. Soc. Rev.*, 2014, **43**, 4824.
- 16 J.-J. Qian, F.-L. Jiang, K.-Z. Su, J. Pan, L.-F. Liang, F.-F. Mao, M.-C. Hong, *Cryst. Growth Des.*, 2015, **15**, 1440.
- 17 W.-T. Liu, H. H. Thorp, *Inorg. Chem.*, 1993, **32**, 4102.
- 18 (a) D. N. Woodruff, F. Tuna, M. Bodensteiner, R. E. P. Winpenny, R. A. Layfield, *Organometallics*, 2013, **32**, 1224; (b) A. S. Chesman, D. R. Turner, S. K. Langley, B. Moubaraki, K. S. Murray, G. B. Deacon, S. R. Batten, *Inorg. Chem.*, 2015, **54**, 792.
- 19 Y. Wang, X.-L. Li, T.-W. Wang, Y. Song, X.-Z. You, *Inorg. Chem.*, 2010, **49**, 969.
- 20 M. L. Kahn, C. Mathonière, O. Kahn, *Inorg. Chem.*, 1999, **38**, 3692.
- 21 J. Goura, R. Guillaume, E. Riviere, V. Chandrasekhar, *Inorg. Chem.*, 2014, **53**,

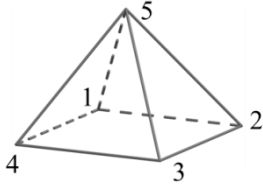
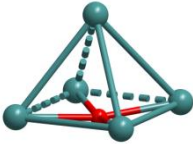
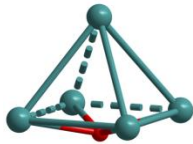
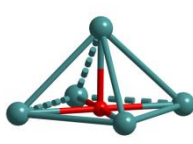
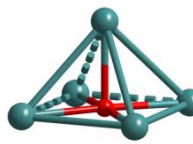
- 7815.
- 22 (a) S. K. Langley, B. Moubaraki, K. S. Murray, *Inorg. Chem.*, 2012, **51**, 3947; (b) J.-B. Peng, X.-J. Kong, Y.-P. Ren, L.-S. Long, R.-B. Huang, L. S. Zheng, *Inorg. Chem.*, 2012, **51**, 2186.
- 23 (a) S. K. Langley, B. Moubaraki, K. S. Murray, *Inorg. Chem.*, 2012, **51**, 3947. (b) Y.-N. Guo, G.-F. Xu, Y. Guo, J.-K. Tang, *Dalton Trans.*, 2011, **40**, 9953.
- 24 P. C. Andrews, F. Hennersdorf, P. C. Junk, D. T. Thielemann, *Eur. J. Inorg. Chem.*, 2014, **2014**, 2849.

Table 1 Crystal data and structure refinement for **1–6**

	1	2	3	4	5	6
Empirical formula	C ₇₄ H ₁₀₅ Cl ₆ Dy ₅ O ₂₄ S ₄	C ₇₄ H ₁₀₃ Cl ₆ Ho ₅ O ₂₃ S ₄	C ₇₄ H ₁₀₃ Cl ₆ Er ₅ O ₂₃ S ₄	C ₁₄₅ H ₁₈₉ Dy ₅ O ₂₆ S ₁₂	C ₁₄₅ H ₁₈₉ Ho ₅ O ₂₆ S ₁₂	C ₁₄₅ H ₁₈₉ Er ₅ O ₂₆ S ₁₂
Formula weight	2532.02	2526.15	2537.80	3545.18	3557.33	3568.98
Crystal system	Triclinic	Triclinic	Triclinic	Monoclinic	Monoclinic	Monoclinic
Space group	<i>P</i> $\bar{1}$	<i>P</i> $\bar{1}$	<i>P</i> $\bar{1}$	<i>C</i> 2/ <i>c</i>	<i>C</i> 2/ <i>c</i>	<i>C</i> 2/ <i>c</i>
<i>a</i> (Å)	16.261(4)	16.251(3)	16.261(4)	55.691(4)	55.685(6)	55.655(3)
<i>b</i> (Å)	17.318(4)	17.345(3)	17.318(4)	15.6952(12)	15.6679(18)	15.6529(8)
<i>c</i> (Å)	19.980(5)	20.033(4)	19.980(5)	41.884(3)	41.807(5)	41.778(2)
α (°)	92.311(4)	92.282(4)	92.311(4)	90	90	90
β (°)	90.557(4)	90.548(3)	90.557 42)	91.9410 (10)	91.872(2)	91.8400(10)
γ (°)	111.324(3)	111.113(3)	111.324(3)	90	90	90
<i>V</i> (Å ³)	5235(2)	5261.7(17)	5235(2)	36589(5)	36456(7)	36376(3)
<i>Z</i>	2	2	2	8	8	8
ρ calc (g/cm ³)	1.606	1.594	1.610	1.287	1.296	1.303
<i>T</i> / K	123(2)	123(2)	123(2)	123(2)	123(2)	123(2)
<i>F</i> (000)	2474	2464	2474	14312	14352	14392
data / restraints / parameters	19504 / 287 / 1100	19725 / 243 / 1090	19543 / 239 / 1090	32311 / 0 / 1961	32186 / 0 / 1961	32119 / 0 / 1961
GOF on <i>F</i> ²	1.035	1.018	1.003	1.062	1.058	1.099
<i>R</i> _{<i>I</i>} ^{<i>a</i>} / <i>wR</i> ₂ ^{<i>b</i>} [<i>I</i> > 2σ(<i>I</i>)]	0.0615 / 0.1769	0.0504 / 0.1430	0.0606 / 0.1711	0.0437 / 0.1291	0.0461 / 0.1196	0.0436 / 0.1234
<i>R</i> _{<i>I</i>} / <i>wR</i> ₂ [all data]	0.0993 / 0.2377	0.0956 / 0.1756	0.1109 / 0.2373	0.0592 / 0.1371	0.0606 / 0.1270	0.0615 / 0.1305

^{*a*} $R_1 = \Sigma||F_o| - |F_c||/\Sigma|F_o|$. ^{*b*} $wR_2 = [\Sigma w(F_o^2 - F_c^2)^2/\Sigma w(F_o^2)^2]^{0.5}$.

Table 2 Selected structure parameters for four Dy₅ pyramids

 pyramid structure	[Dy ₅ (μ ₄ -O)]		[Dy ₅ (μ ₅ -O)]	
	1	[Dy ₅ (μ ₄ -OH)(μ ₃ -OH) ₄ (Ph ₂ acac) ₁₀]	4	[Dy ₅ O(OiPr) ₁₃] ^a
				
space group	<i>P</i> $\bar{1}$	<i>P</i> 4/ <i>n</i>	<i>C</i> 2/ <i>c</i>	<i>C</i> 2
coordinated atoms	O and S	O	O and S	O
symmetry for Dy ₁ –Dy ₅	<i>C</i> _{2v} × 4, <i>D</i> _{4d}	<i>D</i> _{4d} × 5	<i>D</i> _{2d} , <i>C</i> _{4v} , <i>D</i> _{2d} , <i>C</i> _{4v} , <i>D</i> _{3h}	<i>O</i> _h × 5
Dy ₁ ⋯Dy ₃ (Å)	4.982	5.030	4.850	4.596
Dy ₂ ⋯Dy ₄ (Å)	5.023	5.030	5.480	4.917
Dy⋯Dy (Å) ^b	3.766	3.845	3.671	3.671
Dy ₅ ⋯O (Å) ^c	3.046	3.438	2.578	2.404

^a [Dy₅(μ₄-OH)(μ₃-OH)₄(Ph₂acac)₁₀] and [Dy₅O(OiPr)₁₃] from refs 4e and 4f, respectively.

^b Corresponding the average Dy⋯Dy distance between apical Dy₅ ion and four basal Dy^{III} ions.

^c Corresponding the distance between apical Dy₅ ion and the μ₄- (or μ₅-) bridge O atom.

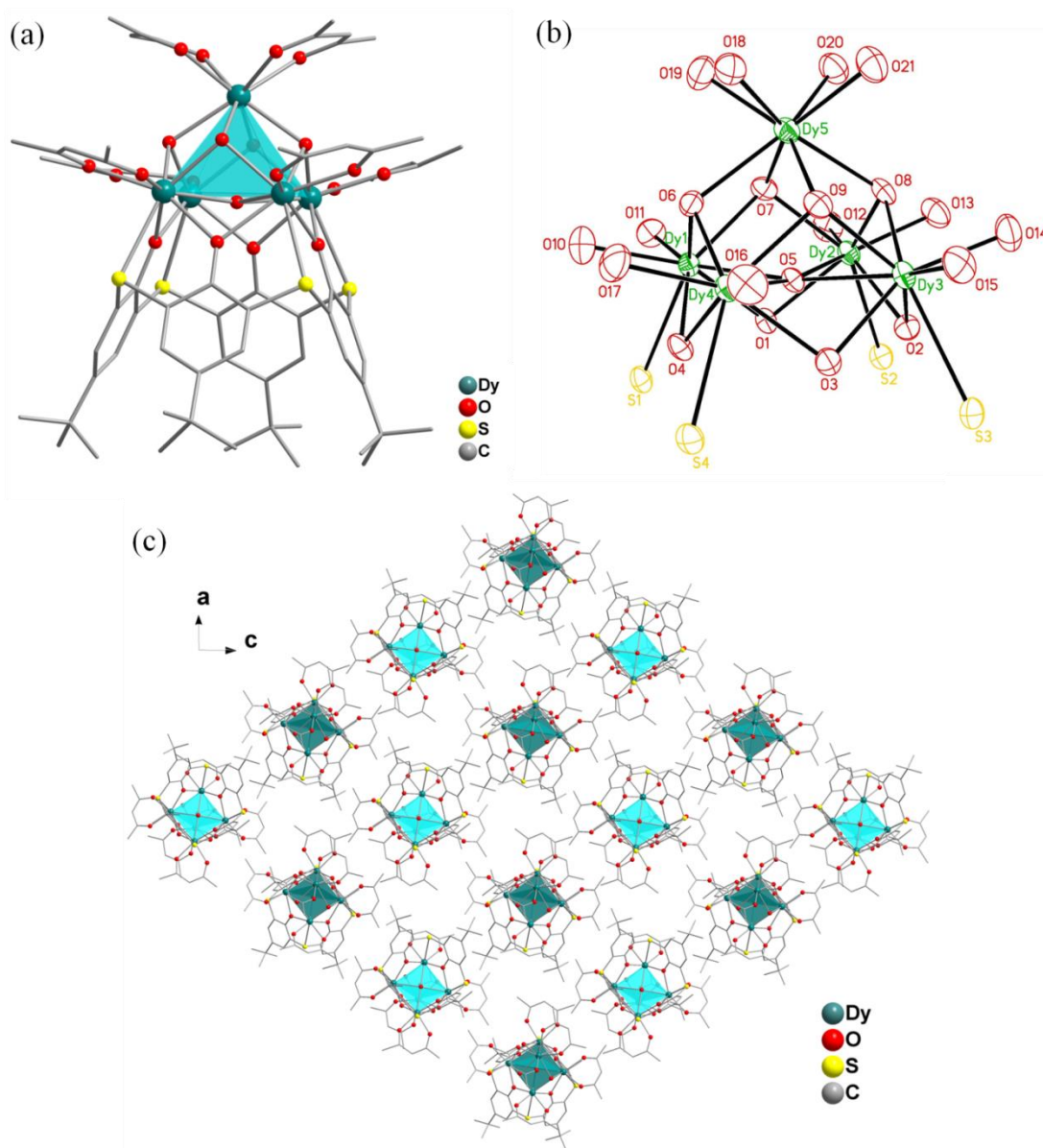


Fig. 1 (a) Pentanuclear structure of complex **1**. H atoms and uncoordinated solvents are removed for clarity. (b) The ORTEP figure of **1**, showing the atom-numbering scheme. Displacement ellipsoids are drawn at the 30% probability level. For clarity, all C atoms and uncoordinated S and O atoms are omitted. (c) The stacking motif of **1**. Solvent molecules are removed for clarity.

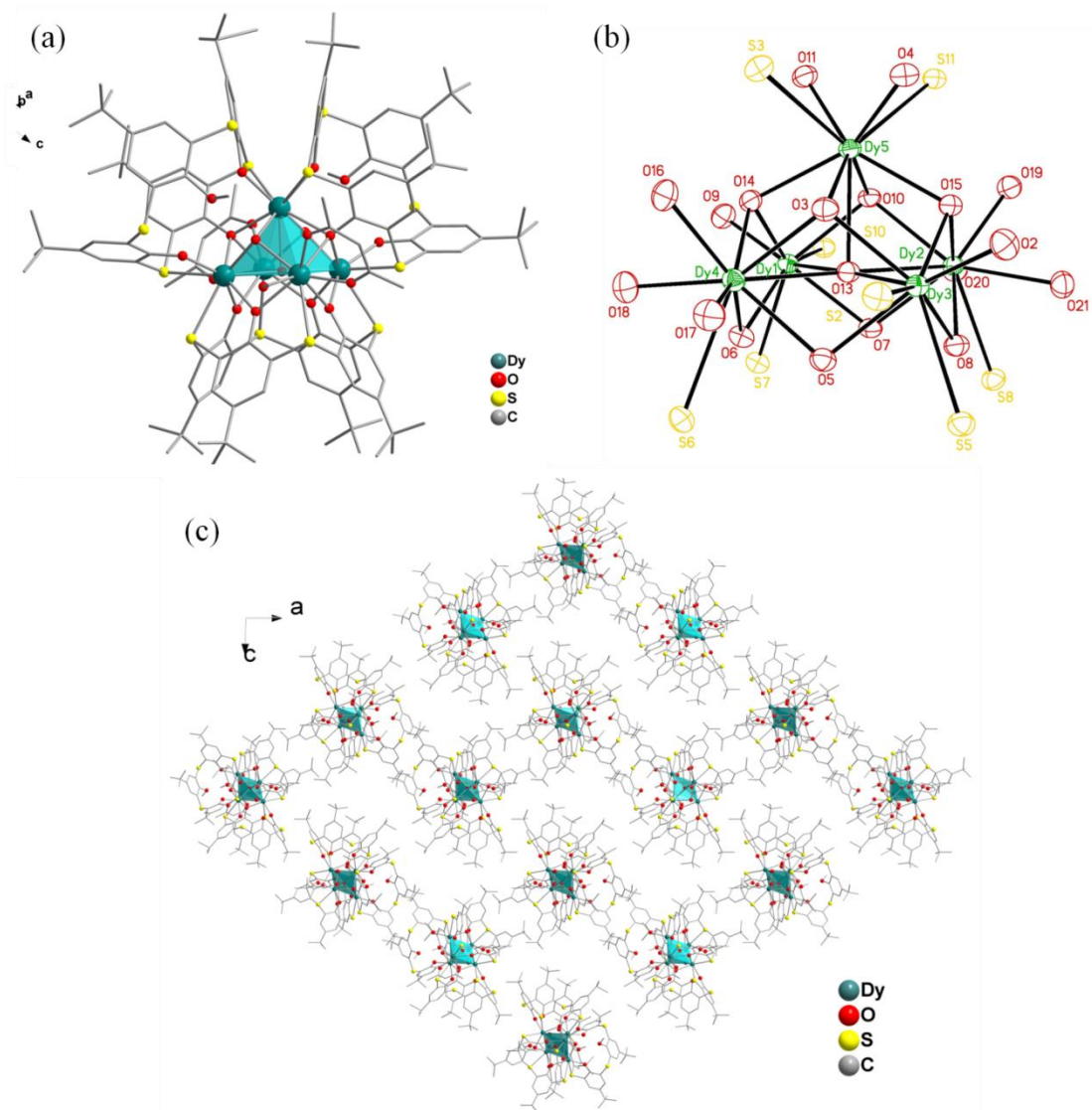


Fig. 2 (a) Pentanuclear structure of complex **4**. H atoms and disordered C atoms are omitted for clarity. (b) The ORTEP drawing of **4**, showing the atom-numbering scheme. Displacement ellipsoids are drawn at the 30 % probability level. For clarity, all C atoms and uncoordinated S and O atoms are omitted. (c) The stacking motif of **4** in the ac plane. Solvent molecules are removed for clarity.

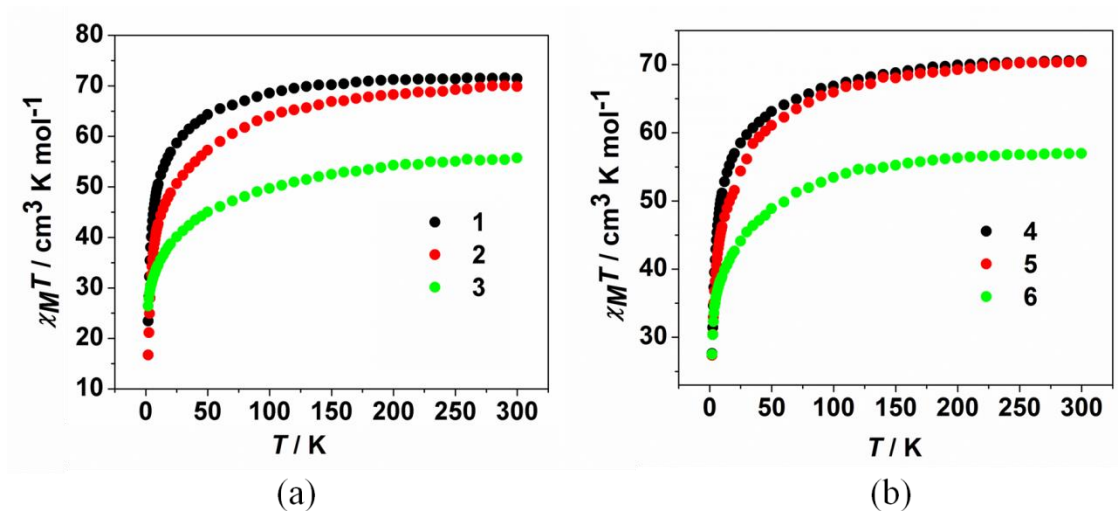


Fig. 3 Temperature dependence of the $\chi_M T$ values for complexes **1–3** (a) and **4–6** (b) in a 1000 Oe field.

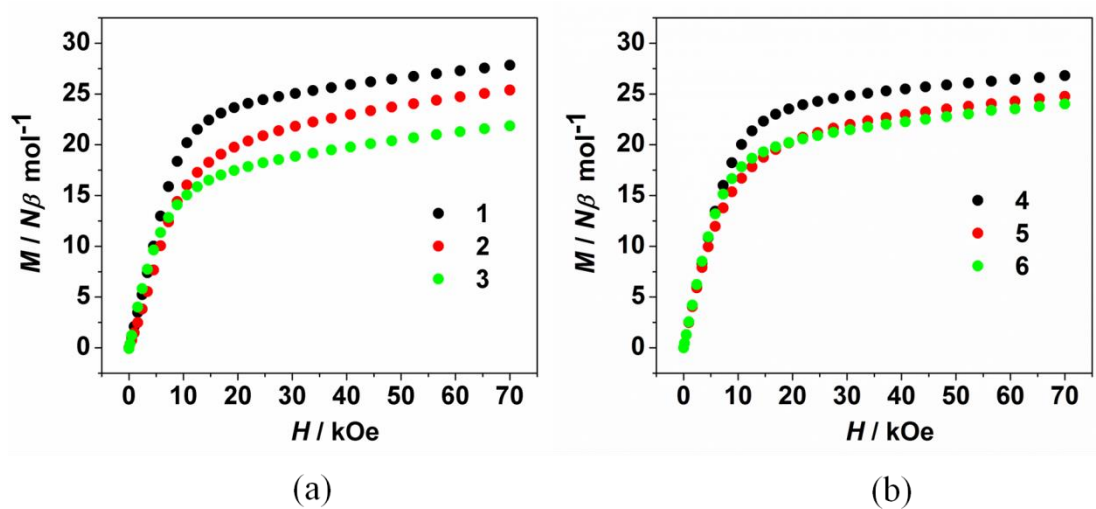


Fig. 4 Field-dependent magnetizations for complexes **1–3** (a) and **4–6** (b) from 0 to 70 kOe at 1.9 K.

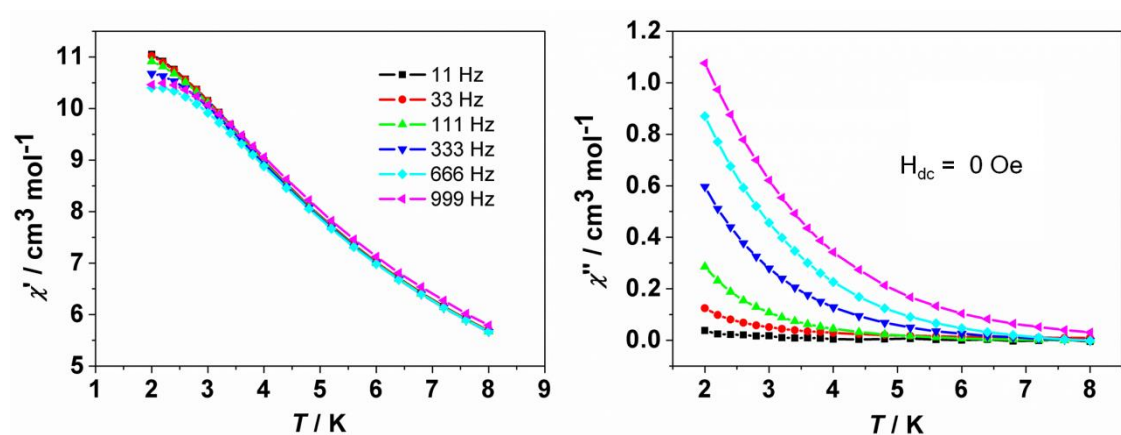


Fig. 5 Temperature-dependent in-phase χ' (right) and out-of-phase χ'' (left) ac susceptibility signals for **1** at the indicated frequencies under zero dc field.

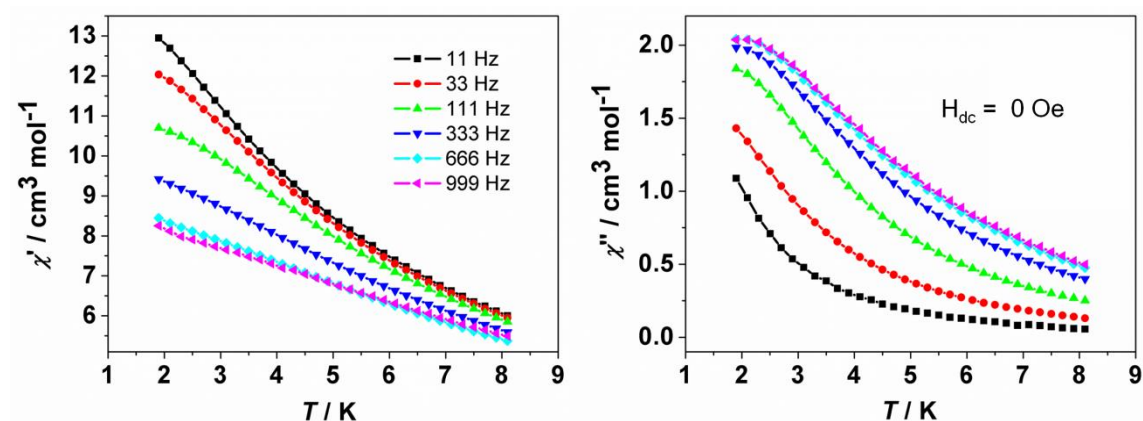


Fig. 6 Temperature-dependent in-phase χ' (right) and out-of-phase χ'' (left) ac susceptibility signals for **4** at the indicated frequencies under zero dc field.